Two experimental tests of a fluctuation-induced first-order phase transition: Intensity fluctuation microscopy at the nematic–smectic-*A* transition

Anand Yethiraj,* Ranjan Mukhopadhyay,† and John Bechhoefer
Department of Physics, Simon Fraser University, Burnaby, British Columbia, Canada V5A 1S6
(Received 1 August 2001; published 16 January 2002)

We have developed a new, extremely sensitive real-space technique (intensity fluctuation microscopy) to probe the order of the nematic–smectic-*A* (*NA*) transition. Using this technique, we show that the *NA* transition in 4′-*n*-octyl-4-cyanobiphenyl (8CB) is clearly first order, contrary to calorimetric studies but in agreement with conclusions drawn from front-velocity measurements. We characterize the strength of the discontinuity at the first-order transition by the dimensionless quantity $t_0=(T_{NA}-T^*)/T^*$. By precisely measuring t_0, we have made the first detailed tests of predictions based on the Halperin-Lubensky-Ma (HLM) theory of fluctuation-induced, first-order phase transitions. First, we explore the effect of an external magnetic field on the *NA* transition. Although modest fields (of order 10 T) are predicted to drive the weakly first-order transition in pure 8CB second order, we observe no such effect; we establish instead that the lower bound on this critical field is $\approx$30 T. Likewise, we observe no effect in mixtures of 8CB with its longer chemical homolog 4′-*n*-decyl-4-cyanobiphenyl (10CB). Second, we examine the dependence of t_0 as a function of 8CB–10CB mixture concentration and find that the data in mixtures with small nematic temperature range are well-fit by the parameters derived by Anisimov *et al.* based on calorimetric measurements. As we increase the nematic range (by using concentrations closer to pure 8CB), the measured t_0 deviates more and more from the HLM predictions. Smectic fluctuations, which are neglected in the HLM calculation, are an obvious candidate to explain such a discrepancy, but one's naive expectation is that they would *reduce* t_0 below the HLM levels, whereas the observed values are too large. However, a recent renormalization-group calculation concludes that smectic fluctuations, surprisingly, should indeed increase t_0, explaining the observations presented here.

DOI: 10.1103/PhysRevE.65.021702 PACS number(s): 64.70.Md, 61.30.Gd, 64.60.Fr

I. INTRODUCTION

One of the most important advances made in our understanding of continuous phase transitions has been the elucidation of how thermal fluctuations modify critical exponents from the values predicted by mean-field theory [1]. But thermal fluctuations have another effect, one that is less-well-understood theoretically and studied only to a limited extent experimentally: when two order parameters are simultaneously present and interact with each other, the fluctuations of the additional order parameter may profoundly alter the phase transition of the underlying system. In high-energy physics, for example, such a situation occurs in the Higgs mechanism [1,2], where the fluctuations of a scalar field can add mass to the soft modes of the underlying transition. In condensed-matter physics, over two decades ago, Halperin, Lubensky, and Ma (HLM) [3] predicted that fluctuations of an additional order parameter could force a system with a second-order phase transition to be first order. They noted two settings where this should occur: the normal-superconducting phase transition in type-1 superconductors and the nematic–smectic-*A* (*NA*) transition in liquid crystals [4]. The importance of fluctuations in soft condensed matter makes the effect observable in the liquid-crystal system, while in superconductors, experiments are well-described by mean-field theory.

Understanding the *NA* transition has been an outstanding problem in condensed-matter physics in its own right [5,6]. Experimentally, the *NA* transition is usually indistinguishable from second order [7]; however, for materials with a small nematic range, calorimetric measurements have detected a small latent heat associated with the phase change, which is interpreted as a mean-field, second-order phase transition that is driven to first order by the coupling to a second, strongly fluctuating order parameter. The second-order parameter is associated with a nearby transition, between the isotropic and nematic phases (*IN*). As described below, the primary order parameter in our case, the *NA* order parameter, is a complex number ψ whose magnitude is proportional to the amplitude of density modulations in the layered smectic phase and whose phase gives the origin in a given coordinate system. The secondary *IN* order parameter, is a symmetric, traceless two-tensor, $Q_{ij}=S(3\hat{n}_i\hat{n}_j-\delta_{ij})/2$, where S describes the degree of nematic ordering and $\hat{n}$ gives the direction of that ordering.

In principle, a complete theory must account for thermal fluctuations in the nematic order parameter magnitude S, the nematic director $\hat{n}$, and the smectic-*A* order parameter ψ. The de Gennes–McMillan mechanism [6] takes into account S fluctuations but is mean field in $\hat{n}$ and ψ. de Gennes [6] and McMillan [8] showed that smectic layering (i.e., a non-

*Present address: FOM Institute for Atomic and Molecular Physics, Kruislaan 407, 1098 SJ Amsterdam, The Netherlands.
†Present address: Department of Physics and Astronomy, University of Pennsylvania, 209 South 33rd St., Philadelphia, PA 19104-6396

 ©2002 The American Physical Society

zero ψ) could increase orientation ordering from its normal value S to $S+\delta S$. The δS-ψ coupling can then drive first order a transition that would otherwise be second order, but it does so by adding a negative term to the quartic coefficient of the Landau free energy expansion in the smectic-A order parameter ψ. This term is large when T_{NA} is close to T_{IN}, so that reducing the width of the nematic range of one's system (e.g., by altering the concentration of a binary mixture), one can drive the transition first order. The δS-ψ coupling changes the values of coefficients in the Landau free energy expansion but does not add any new terms to the series.

A more subtle mechanism, proposed by Halperin, Lubensky, and Ma (HLM) [3,4], takes into account the coupling between ψ and the nematic director fluctuations $\vec{\delta n}$. Here, the projection of the two-parameter free energy back onto a free energy depending only on ψ is done by integrating out the nematic director fluctuations, assuming that the smectic fluctuations are very slow on this time scale. The theory treats the nematic fluctuations in the Gaussian approximation but is mean field in ψ. This new coupling, although weak, alters the analytic structure of the free energy, introducing in effect a negative cubic term that ensures that the transition is always at least weakly first order. Such a term was initially excluded from the free-energy expansion, whose structure has thus been profoundly altered by the thermal fluctuations.

Experimental studies in the small-nematic-range limit [9] were carried out by various groups [10–15]. Systematic measurements of the latent heat as a function of T_{NA}/T_{NI} were possible because one can tune the nematic range by mixing two almost-similar liquid crystals with slightly different aliphatic chain lengths. In the de Gennes–McMillan theory (i.e., taking only the δS-ψ coupling into account), the latent heat should vary linearly with $\delta x = x - x^*$, for small δx, where x is the mixture concentration and x^* is the concentration where the latent heat vanishes and is thus, in the context of this Landau theory, a tricritical point. By convention, x^* is known as the Landau tricritical point (LTP). Brisbin *et al.* [10] and Thoen *et al.* [11] showed that this is true well above x^*. Reanalyzing data [13] from mixtures of two cyanobiphenyl liquid crystals in a homologous series, 8CB and 10CB, Anisimov *et al.* [14] showed that the latent heat did not go to zero at the LTP but crossed over nonlinearly to a measurable, nonzero value. This indicated that something other than δS-ψ coupling was also important, and Anisimov *et al.* showed that the experimental results were at least consistent with the HLM predictions. Tamblyn *et al.* [16,17] demonstrated a similar dependence via capillary length (ratio of the surface tension to the latent heat) measurements on 8CB–10CB mixtures.

In addition, Cladis *et al.* introduced a different technique for studying weakly first-order transitions. They measured the propagation speed of a *NA* front after a step jump in temperature. The velocity was a linear function of the temperature jump ΔT. For second-order transitions, the front propagation speed should be proportional to $\Delta T^{1/2}$. This result implied that the *NA* transition was first order for all 8CB–10CB mixtures, including pure 8CB.

Although these previous experiments have clearly indicated the importance of fluctuations effects close to the LTP, they can barely probe the precise predictions of the HLM theory. In the present article, we shall introduce a more sensitive experimental technique that, while consistent with the larger error bars of previous experiments, shows clear deviations from the HLM predictions. One innovation is to express the current and previous measurements in terms of a common quantity, $t_0 = (T_{NA} - T^*)/T^*$, where T_{NA} is the equilibrium *NA* transition temperature. T^* is the spinodal temperature, where the nematic phase would become unstable. One can measure T^* via almost any physical quantity by extrapolating to the temperature at which critical effects diverge. Because t_0 is positive for a first-order transition and zero in a second-order transition, it is a useful dimensionless measure of the strength of a first-order transition.

We present two experiments:

(i) We probe the effect of an external magnetic field H on the fluctuation-induced first-order discontinuity of the *NA* transition: i.e., we measure $t_0(H)$. A strong-enough magnetic field is predicted to drive the *NA* transition back to second order. We shall show that external-field effects are much weaker than predicted by HLM.

(ii) We repeat previous experiments on binary mixtures of 8CB and 10CB, where the nematic range varies with mixture concentration x; i.e., we measure $t_0(x)$. Although previous work found results consistent with HLM, our more precise measurements show a clear deviation.

A letter describing part of this work was published earlier [18]. More experimental details may be found in Ref. [19].

The plan of the article is as follows: In Sec. II, we summarize the effect of an external field on the HLM mechanism [20]. In Sec. III, we describe and characterize a new high-resolution real-space method, intensity fluctuation microscopy (IFM), which we developed for this study. In Sec. IV, we use IFM to measure the discontinuity t_0 at the *NA* transition in 8CB and 8CB–10CB mixtures and in the presence of an external magnetic field. Finally in Sec. V, we summarize our results and present directions for future work.

II. THE "HALPERIN-LUBENSKY-MA" EFFECT IN THE PRESENCE OF AN EXTERNAL FIELD

A. Review of the zero-field calculation

Here, we briefly sketch the results of the HLM calculation. For a more thorough discussion, see, for example, the book by de Gennes and Prost [6]. The smectic order parameter may be defined as the first coefficient in the Fourier expansion of the periodic density fluctuations,

$$\rho(z) = \rho_0[1 + \mathrm{Re}(\psi e^{iqz})], \tag{1}$$

where the amplitude of the complex number $\psi = \Psi e^{i\Phi}$, with Ψ the magnitude of density fluctuations and Φ their phase. Because the phase origin is arbitrary, the free energy must be a function of $|\psi|$ alone.

Assuming that $\hat{\mathbf{n}}$ fluctuates about the z axis, one can write the free energy as [6]

$$F_{NA}(\psi,\delta\mathbf{n})=\int d^3x f_{NA}(\psi,\delta\mathbf{n})=\frac{1}{2}\int d^3x r'|\psi|^2+\frac{u'}{2}|\psi|^4 + C_{\parallel}\left|\frac{\partial\psi}{\partial z}\right|^2+C_{\perp}|(\boldsymbol{\nabla}_{\perp}-i\mathbf{q}_0\cdot\delta\mathbf{n}_{\perp})\psi|^2 + K_1(\boldsymbol{\nabla}\cdot\delta\mathbf{n}_{\perp})^2+K_2(\hat{\mathbf{z}}\cdot\boldsymbol{\nabla}\times\delta\mathbf{n}_{\perp})^2 + K_3\left(\frac{\partial}{\partial z}\delta\mathbf{n}_{\perp}\right)^2, \quad (2)$$

where $\delta\mathbf{n}_{\perp}=(\delta n_x,\delta n_y,0)$. We assume that close to the transition, r' is of the form $\alpha'(T-T_0)/T_0$, where α' is temperature independent. Also, $q_0=2\pi/d$ is proportional to the reciprocal of the smectic layer spacing d, $C_{\parallel}$ and $C_{\perp}$ set the ''rigidity'' of smectic fluctuations, and the Frank constants K_1, K_2, and K_3 are the splay, twist, and bend elastic constants for nematic fluctuations. To simplify slightly the free energy, we will at different times consider either the limit of equal elastic constants K or the somewhat more realistic limit that K_2 and K_3 are much larger than K_1.

The idea of HLM was that in the ''type-I'' limit (which, physically, corresponds to small nematic range), the nematic fluctuations are stronger than the smectic ones and may be integrated out, yielding an effective free energy of the form

$$f_{NA}(\psi)=\frac{1}{2}r|\psi|^2+\frac{1}{3}w|\psi|^3+\frac{1}{4}u|\psi|^4+\frac{1}{6}E|\psi|^6, \quad (3)$$

where the coefficients r and u (and α) have been renormalized and where there is a qualitatively new term, $\sim|\psi|^3$, whose coefficient

$$w=-\frac{k_BT}{\pi}\frac{C_{\perp}^{3/2}q_0^3}{4K_3^{1/2}}\left(\frac{1}{K_3}+\frac{1}{K_2}\right), \quad (4)$$

valid in the limit $K_1\to 0$. Because of the cubic term w, the transition is first order. Because w is small, the first-order discontinuity is weak. The size of the discontinuity is then

$$t_0=\frac{2}{9}\frac{w^2}{\alpha u}. \quad (5)$$

The presence of the $|\psi|^3$ term in Eq. (3) does not violate any symmetry, since it involves only the magnitude of ψ. The original expansion, Eq. (2), does not contain such terms because they would violate the analyticity assumed in an expansion. However, nothing prevents such terms from being present in an *effective* free energy, derived by integration over fluctuation terms in the original expansion.

B. Effect of an applied magnetic field

Adding a magnetic field H along the z axis leads to an additional term in the free energy,

$$F_{NA}^H=F_{NA}+\int d^3x\frac{1}{2}\chi_a H^2\delta n_{\perp}^2. \quad (6)$$

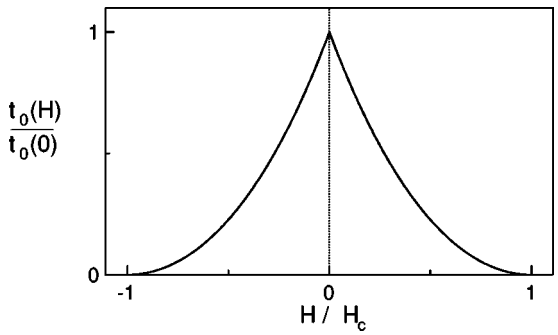

FIG. 1. Reduced temperature $t_0=(T_{NA}-T^*)/T_{NA}$ as a function of the scaled magnetic field H.

In the zero-field case, massless nematic director fluctuations, by coupling to the smectic order parameter, induce a first-order transition. Adding a magnetic (or electric) field adds mass to these director fluctuations, thus suppressing their effect. When the magnetic field is strong enough, director fluctuations can be ignored, and we get an XY-type second-order transition. The length scale over which nematic twist and bend distortions are expelled by the smectic phase is the penetration length λ, which, in a mean-field calculation (and in the one-constant approximation $K_1=K_2=K_3=K$) is given by

$$\lambda=\left(\frac{K}{C}\right)^{1/2}q_0\psi_0. \quad (7)$$

Adding a field introduces a new length, the magnetic coherence length, which is a measure of the distance over which twist, bend, or splay excitations decay in the nematic phase. In our notation, the magnetic coherence length is given by

$$\xi(H)=\left(\frac{K}{\chi_a}\right)^{1/2}\frac{1}{H}. \quad (8)$$

As long as $\xi(H)\gg\lambda$, the nature of the nematic-smectic interface remains unmodified. On the other hand, when $\xi(H)\lesssim\lambda$, nematic fluctuations are sufficiently suppressed in both the nematic and smectic phases, and play no role at the transition. A rough estimate of magnetic field H_c needed to reach the tricritical point can be obtained by setting $\xi(H_c)=\lambda$. In reality, the different values for K_1, K_2, and K_3 give rise to different penetration depths and magnetic coherence lengths for the bend and the twist modes. A more careful calculation gives

$$H_c=\left[\frac{9}{8}\frac{\alpha}{u}\frac{C_{\perp}q_0^2}{\chi_a}\right]^{1/2}\left(1-\frac{b}{2}\right)\sqrt{t_0}\equiv H_0\sqrt{t_0}, \quad (9)$$

where H_0 is a scale field that depends on known material parameters and $b=K_2/(K_2+K_3)$. For 8CB, $H_0\approx 3500$ T. Using the experimental value $t_0\approx 10^{-5}$ (see Sec. IV), we find a critical field of $H_c\approx 10-15$ T. Further analysis of the field effects show that the initial decrease in $t_0(H)\propto|H|$, where the nonanalytic cusp at $H=0$ again reflects the altered analytical form of the effective free energy (see Fig. 1).

III. REAL-SPACE MICROSCOPY OF NEMATIC DIRECTOR FLUCTUATIONS

A. Motivation

In the HLM theory, the order parameter of the low-temperature phase (e.g., superconductor or smectic-*A*) couples to a ''gauge field'' (vector potential for the superconductor, director for the smectic-*A*) whose fluctuations diverge at long wavelengths. Measuring director fluctuations at long length scales should then be a very sensitive probe of fluctuation effects at the *NA* transition. Light scattering is the traditional tool for probing fluctuation effects; however, at long length scales (small q), the scattered light is concentrated in small angles with respect to the forward beam and requires care to separate it from the unscattered light. By contrast, in real space, it is easy to probe long length scales. (In practice, the sample thickness acts as a long-scale cutoff.) The idea then is to measure, in real space, the director fluctuations as the temperature is lowered towards the smectic-*A* phase. In the smectic-*A* phase, twist and bend fluctuations are ''expelled,'' while splay fluctuations correspond to layer bending and are allowed. One therefore expects that long-wavelength director fluctuations should be significantly reduced in the smectic-*A* phase. For a first-order *NA* transition, there should be a discontinuity in the fluctuations at the transition.

To visualize director fluctuations, we note that all macroscopic quantities in the nematic phase, including the refractive index, are tensorial quantities that share the symmetry of the nematic order parameter. Thus an undistorted uniaxial nematic is uniaxially birefringent, and a unidirectional, planar-anchored nematic behaves as a waveplate, with optic axis along the average director orientation. When this liquid-crystal waveplate is placed between crossed polarizers and light is passed through it, the director fluctuations give rise to local fluctuations of the average intensity. For incident light parallel to the optic axis, the intensity varies as a function of the angle θ between polarizer and optical axis as

$$I(\theta) = I_0 \sin^2 2\theta \sin^2(\gamma L/2), \tag{10}$$

where I_0 is the transmitted intensity at $\theta = 0$ and $\gamma = 2\pi(\Delta n)/\lambda$ is the mean phase retardation or length produced by the birefringence $\Delta n = n_\perp - n_{||}$ of the nematic as light crosses the sample thickness L. Here, $n_{\perp,||}$ are the indices of refraction for light polarized perpendicular and parallel to the local director orientation. Near $\theta = \pi/8$, $I(\theta)$ is linear, and intensity fluctuations are linearly related to director fluctuations. Of course, the above discussion ignores out-of-plane fluctuations and assumes the illumination to be perfectly normal to the sample plane. In Appendix A, we describe the optics of the fluctuating nematic in more detail. We reported earlier on a preliminary version of this technique [21]. A similar method was independently developed by Galerne *et al.* to make quantitative elastic-constant measurements [22].

B. Sample preparation

Samples were prepared between glass slides or glass cubes. The surfaces bounding the liquid crystal were treated for unidirectional planar anchoring. Two methods of anchoring were used successfully: one involved oblique-angle SiO evaporation, the other unidirectional rubbing of a polyimide layer coated onto the glass substrate. The glass slides were 1 mm thick microscope slides or 2 mm thick ITO-coated slides, all cut to a size of $\simeq 15$ mm$\times 15$ mm. The cubes were 12.7 mm$\times 15$ mm$\times 15$ mm. The liquid crystal occupies the space between the slides or cubes, whose thickness was set and parallelism measured interferometrically to be constant to within 0.5 μm across the extent of the sample. Typical sample thicknesses ranged from 7.5 to 30 μm.

We used the liquid-crystal 4′-*n*-octyl-4-cyanobiphenyl (8CB) and its slightly longer homolog 4′-*n*-decyl-4-cyanobiphenyl (10CB) [23]. Each of these is a well-studied material, with the relevant material parameters already known; in addition, the binary phase diagram has been previously measured [13]. Above a 10CB concentration of about $x = 0.6$ mol%, there is only a smectic-*A*–isotropic transition; below this triple point, one finds a nematic phase, whose coexistence range increases as one decreases the concentration x of 10CB.

Because the main contaminant (0.1–0.2 mol%) is water, we purified each liquid crystal in a hot stage whose temperature was set slightly above the *IN* transition and whose pressure was maintained at 50 mtorr. The more volatile water vapor is pumped away, and the bubbling subsides after about 15 min.

C. Setup

The setup used a home-built microscope with a working distance ≈ 5 cm. The illumination for the microscope was provided by a xenon flashlamp [24], which was coupled by a meter-long optical fiber. The glass fiber absorbs infrared radiation that might perturb the liquid-crystal temperature; in addition, the multimode fiber scrambles the azimuthal structure of the xenon source, leading to a more homogeneous illumination field [25]. Images of the planar-anchored nematic sample were taken between crossed polarizers by a 12-bit digital CCD camera [26].

The sample was temperature controlled in a home-built gradient hot stage. The hot-stage was designed to control independently the temperature of the top and bottom of the sample and thus impose a variable gradient across the sample. The sample plane was vertical in the laboratory frame of reference. The high thermal mass of the copper blocks in the sample holder enhanced the short-time stability, while rms fluctuations in temperature over long times (≈ 1 h) were roughly 0.15 mK, they were less than 0.05 mK over the duration (a few seconds) of a measurement. Each control loop used its own separate Peltier element. The far side of each was thermally linked to a waterbath whose temperature control was stable to 10 mK [27]. The Peltier elements then provided fine regulation by pumping heat to and from the sample. The Peltier current was provided by a computer-controlled power supply [28], whose output was updated once per second according to a proportional-integral-derivative (PID) algorithm whose input was provided by a voltage measured across a Wheatstone bridge that

was itself kept in a box regulated to ± 100 mK. The bridges were powered by silver-oxide batteries to reduce external noise. Two arms of each bridge were fixed resistances; for the other two, one was a fixed resistor in series with a tunable potentiometer, while the other was a 2000-Ω-platinum RTD sensor, which was thermally as close as possible to the sample. Temperature differences across the sample field of view could be varied from 20 mK to about 500 mK without changing the water-bath control temperatures.

D. Calibration of temperature gradient

In general, we imposed a small temperature gradient in the plane of the sample. The gradient was aligned so that it lay along an image row. We then measured fluctuations by averaging over each pixel column, along the isotherm. The advantage of this trick is that small temperature gradients mean that each column corresponds to a small temperature range (10 to 100 μK). We then have an easy way of ''scanning'' the temperature, simply by processing the data from each column separately. Also, as we shall see below, having data that crosses the *NA* transition allows us to fix the phase-transition temperature much better.

To calibrate this temperature gradient, we increased by a common amount the set point of both control loops and observed the proportional shift of the interface. The plot of the interface position varied linearly with temperature, implying that the temperature gradient is linear, too. Typical gradients ranged from 0.1 to 1 K/cm and were sufficiently uniform that the image of the interface on the CCD was flat.

E. Characterization of IFM

1. The variances $\hat{\zeta}$ and ζ

The main step in IFM is to estimate the variance of intensity fluctuations on the length scale of a CCD pixel. Consider two images of the fluctuating planar nematic. If the exposure time is less than the characteristic time of fluctuations on a length scale set by one pixel, then each image can be considered a ''snapshot'' of the fluctuations. In our case, the xenon flashlamp gave an effective exposure time of about 10 μs, much faster than fluctuations on the 1-μm pixel scale (about $l^2\gamma_{rot}/K \approx 1$ ms, where $l \approx 1$ μm is the length scale of a pixel, $\gamma_{rot} \approx 0.1$ P is the viscosity of the nematic, and $K \approx 10^{-6}$ dyn is a typical nematic elastic constant). If the time interval between the two pictures is longer than the longest relaxation time scale, then the fluctuations in each snapshot will be independent. (This time scale is roughly $L^2\gamma_{rot}/K \approx 1$ s, where L is the sample thickness, typically 30 μm). Taking the difference between the two images removes any illumination variations and nonuniformities and constant offsets in the CCD response, leaving fluctuations whose mean is very close to zero. Because each individual pixel is in effect an independent measurement, we can construct an ''ensemble average'' over the 1.3 million pixels in the difference image. Averaging over pixels rather than time minimizes temperature drifts during the measurement, which is crucial here.

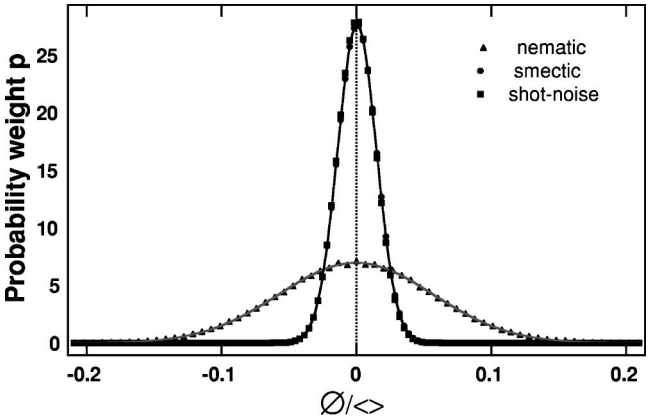

FIG. 2. Probability distribution functions in the nematic and smectic-*A* phases, and in a blank field. Solid lines are fits to Gaussians. Image is 640×480 pixels.

The probability distribution of fluctuating intensities is a Gaussian whose mean is, by construction, close to zero see (Fig. 2). Its variance is

$$\hat{\zeta} = \langle \delta I^2 \rangle - \langle \delta I \rangle^2, \tag{11}$$

where $\delta I(x,y) = I_1(x,y) - I_2(x,y)$ is the difference of the two images and where the variance is calculated over the set of pixels in the difference image that are at the same temperature. Ideally, $\langle \delta I \rangle = 0$, but, in practice, small variations in the flashlamp intensity, etc., led to a (barely) detectable mean in the difference image. Figure 2 shows the distribution of fluctuation intensities in the nematic and smectic-*A* phases, as well as in a blank field (with no sample, and the polarizers uncrossed) where the primary contribution to the fluctuation signal comes from the photon shot noise. This noise is unavoidable as it comes simply from random counting statistics of the photons that impinge on each CCD pixel. In the nematic, where the director fluctuations are a soft mode, $\hat{\zeta}$ is large and decreases as the temperature is reduced. In the smectic-*A* phase, $\hat{\zeta}$ is not noticeably higher than the noise level. The variance of the shot noise is Poissonian, $\hat{\zeta}_{SN} \propto I_0$, while the nematic intensity fluctuations scales as I_0^2, where I_0 is the incident light intensity [29].

The raw variance in the smectic-*A* is indistinguishable from the shot-noise background. This is a bit surprising at first, because the splay elastic constant in the nematic does not diverge at the *NA* transition. The smectic bend mode (which corresponds to the nematic splay mode) in the nematic should then still contribute to the fluctuations; however, the unidirectional planar anchoring in thin samples tends to suppress the splay mode, making this technique more sensitive to the twist and bend modes, especially for thinner samples.

2. Dependence of $\hat{\zeta}$ on the incident light intensity

In order to separate the shot noise from the director fluctuations, which both obey approximately Gaussian distributions of zero mean, we use their different dependencies on

intensity. The variance of shot noise is linear in the intensity, while that due to the liquid-crystal contribution is expected to be quadratic.

When the relation between the angular fluctuations and the intensity fluctuations is linear, one need not independently measure the incident light intensity, as it is proportional to the average transmitted intensity. The average light intensity can be estimated by the average over the two frames captured, for each pixel: i.e., $\overline{I}(x,y)=\frac{1}{2}[I_1(x,y)+I_2(x,y)]$. This average can of course be improved by collecting more images, at the expense of greater susceptibility to temperature drifts. Because any illumination variance is long wavelength, one can construct an average from just two images by further averaging spatially over $\simeq 10\times 10$ pixels. This was found to be necessary only when the illumination intensity variation across the field-of-view was larger than 10%. When well aligned, our optical system gave a 7–10% intensity variation, mostly along the radial direction.

The shot-noise background is calibrated using a blank field, with no liquid-crystal sample. The angle between the polarizer and analyzer is varied to set the transmitted light intensity. In Fig. 3, we show the variance of nematic and blank-field data as a function of the average transmitted intensity. The blank-field data in Fig. 3(a) is well fit by a straight line with a nonzero intercept for most of the range of intensities. The intercept of the blank-field curve places the zero-light offset at 63.7 ± 0.1 gray levels. This offset includes dark noise (negligible) and read noise (1.8 gray levels).

When the liquid-crystal sample is added, the variance is fit well by a quadratic function. Note that the fit shown is *not* a best fit to three free parameters (constant, linear, and quadratic coefficients) but rather is a fit with the offset and linear term held at the shot-noise values. This *raw* signal variance has in it a shot-noise contribution as well. Since the signal variance and shot-noise variance are statistically independent, and since both distributions are Gaussian, we may subtract $\hat{\zeta}_{SN}$ from $\hat{\zeta}$ to isolate the signal variance. Because the signal variance increases quadratically and the shot-noise linearly with average intensity, the signal-to-noise ratio increases linearly with average intensity. The normalized variance

$$\zeta=\frac{\hat{\zeta}-\hat{\zeta}_{SN}}{(\langle\overline{I}\rangle-I_{offset})^2} \tag{12}$$

is then independent of the incident light intensity, as shown in Fig. 3(b). For lower light levels, the denominator in this expression becomes small, giving rise to systematic errors in determining ζ. In our measurements of t_0 for the *NA* transition, we use ζ, measured with sufficient intensity, as our measure of the nematic fluctuations.

3. Dependence of $\hat{\zeta}$ on the incident light polarization angle

In the previous section, the incident light was polarized at $\theta=\pi/8$ with respect to the director, and we assumed that there was a linear relation between angular fluctuations of the director and the corresponding intensity fluctuations. In this linear approximation, one expects that the intensity

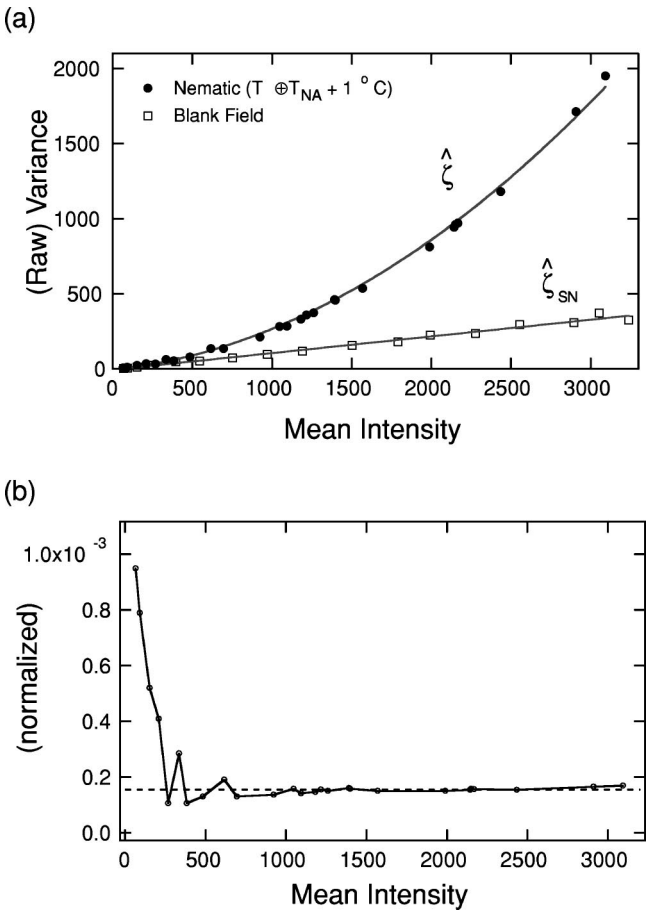

FIG. 3. (a) The variance of the shot noise $\hat{\zeta}_{SN}$ as a function of the mean intensity $\langle I\rangle$ is linear, with a slope of 0.111 ± 0.003. The reciprocal of the slope gives the camera's sensitivity, 9.0 ± 0.2 photoelectrons/gray level. The variance of the signal [top curve in (a)] is quadratic. (b) The normalized variance ζ is independent of mean intensity for intermediate and high light levels. See text.

maxima and minima ($\theta=0, \pi/4, \pi/2, \ldots$) should be minima for the fluctuations; they should be largest where the mean intensity variation with angle is linear (near $\theta=\pi/8$, etc.). Here, we are implicitly approximating the optics of the nematic to be a fluctuating waveplate, where in-plane fluctuations dominate while out-of-plane fluctuations are higher order and are ignored. In this highly simplified approximation, the fluctuation variance (not normalized by the intensity)

$$\hat{\zeta}\propto\left[\frac{d\langle I\rangle}{d\theta}\right]^2\propto\sin^2 4\theta, \tag{13}$$

where $\langle I\rangle\propto\sin^2 2\theta$ is the mean intensity and θ is the angle between the sample optic axis and one of the polarizers.

Figure 4(a) shows that the mean intensity follows the expected form; however, we do not observe $\hat{\zeta}\propto\sin^2 4\theta$. An additional $\sin^2 2\theta$ term is required [Fig. 4(b)]. Intuitively, such a term can arise from out-of-plane fluctuations, which should follow the same angle dependence as the mean intensity. However, because the intensity varies quadratically with out-of-plane fluctuations, one would expect such a term to be

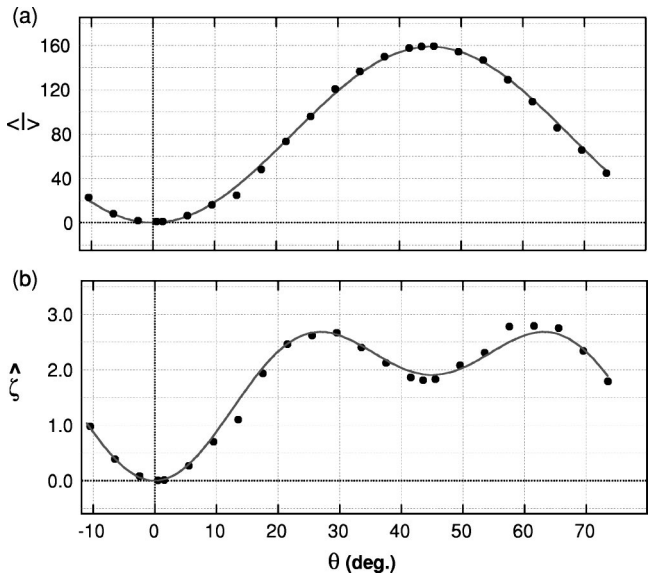

FIG. 4. Mean intensity and variance as a function of θ. (a) Mean Intensity is fit to $a_1 \sin^2 2\theta$, with $a_1 = 158.6 \pm 0.8$. (b) Raw Variance (shot-noise subtracted) is fit to $a_2 \sin^2 4\theta + b_2 \sin^2 2\theta$, with $a_2 = 1.58 \pm 0.05$ and $b_2 = 1.91 \pm 0.05$.

small (second order). In Appendix A, we argue that the contribution of out-of-plane fluctuations is higher than one might expect because the microscope collects rays that propagate at an angle with respect to the optical axis.

4. Dependence of ζ on the sample thickness

The thickness of the liquid-crystal sample also introduces nonideal optical effects in the data. To explore these, we prepared a wedge sample with wire spacers 12.5 and 50 μm thick. We then analyze the variance and mean intensity along strips of equal thickness, in effect scanning as a function of thickness. We inserted an interference filter ($\lambda = 546 \pm 5$ nm) to have quasimonochromatic light. Ordinarily, our observations were in white light to maximize the intensity and to minimize the kinds of birefringence effects discussed here.

Both the mean intensity and normalized fluctuations (Fig. 5) oscillated with thickness. Successive maxima are spaced by a distance corresponding to a thickness variation of $\Delta L = 4.4$ μm. From Eq. (10), we expect $\langle I(L) \rangle \propto \sin^2 \gamma L/2$, which implies $\Delta L = \lambda / \Delta n$, where Δn is the nematic birefringence. We find $\Delta n = 0.12 \pm 0.01$, which is close to the value $\Delta n \approx 0.14$ expected from independent measurements of the refractive indices in 8CB by Karat and Madhusudana [30]. The oscillations decrease with thickness, suggesting that multiple-scattering effects are important for thicker samples and implying that the sample thickness should be kept much less than 50 μm.

To choose an optimal sample thickness, one must balance opposing constraints. Minimizing multiple scattering favors thinner samples. Thinner samples also minimize the effects of any stray vertical temperature gradients. On the other hand, below about 20 μm, surface defects will begin to be imaged, and their static variation will contribute more and

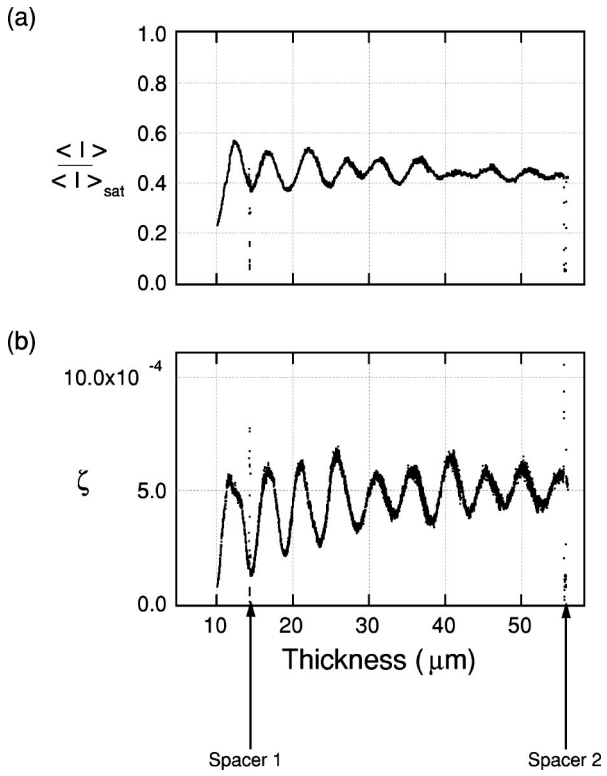

FIG. 5. The thickness dependence of the mean intensity and the normalized fluctuations in the wedge sample. (a) Mean intensity, normalized to the saturation value of the CCD. (b) Normalized fluctuations.

more to $I(x,y)$. These variations can be mostly eliminated by taking a difference image. Our samples then had thicknesses ranging from $L = 7.5$ to 30 μm, over which there was no systematic variation in t_0 with sample thickness, Sec. IV B.

5. Dependence of ζ on the temperature gradient

One might wonder whether the applied temperature gradient affects the measurements of t_0. Experimentally, the gradients we applied ranged from 0.1 to 1 K/cm, and we saw no systematic variation of t_0 with gradient. We also conducted a number of constant-temperature measurements, which agreed with the values extracted in a gradient. Indeed, previous ''constant-temperature'' experiments have had uncontrolled gradients ≈ 0.1 K/cm.

We argue that all of this is not surprising; in a first-order phase transition (unlike a second-order one), there are natural temperature and length scales associated with the transition, given by $T_{NA} - T^*$ and by the maximum correlation length ξ_0 (that is, evaluated at T_{NA}). Their ratio defines a natural gradient scale G^*. For smaller gradients, the adiabatic approximation we use is justified; larger gradients would tend to suppress the first-order discontinuity. For 8CB, we measure $T_{NA} - T^* = 3.7$ mK (see below) and from [31], one estimates that at T_{NA}, $\xi_0 = 0.065$ μm perpendicular to the director and 0.89 μm parallel to the director. Since we used a geometry where the director was perpendicular to the temperature gradient, the first length is the relevant one, giving $G^* = 570$ K/cm. (The other geometry would give G^*

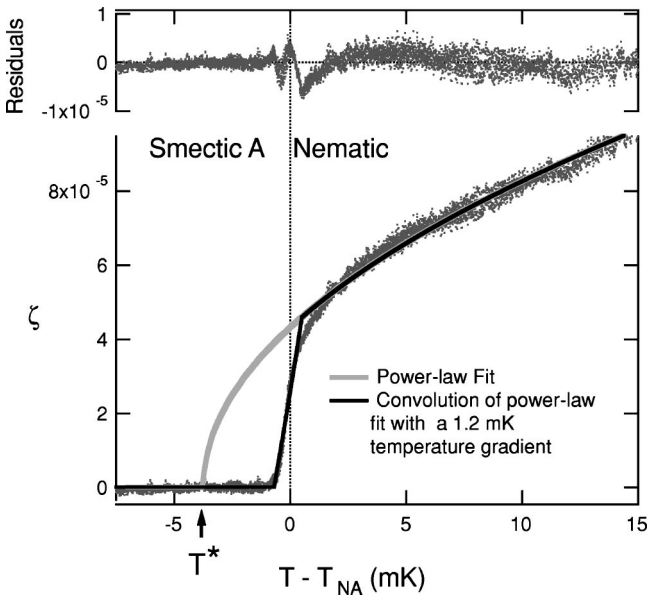

FIG. 6. The fluctuations in the nematic, fit between points A and B by a power law with exponent $\bar{\nu}=0.5$. The extrapolated divergence temperature (spinodal point) is T^*, while the actual transition occurs at T_{NA}. We also show the fit and residuals to a power law convolved with a kernel corresponding to a vertical temperature gradient. Data averaged from 16 images of a pure 8CB sample, $L=7.5$ μm and $G=0.17\pm0.01$ K/cm.

$=42$ K/cm.) The actual gradients we applied were two to three orders of magnitude smaller than these.

IV. REAL-SPACE MAGNETIC-FIELD STUDIES IN PURE 8CB AND 8CB–10CB MIXTURES

Here, we describe our main experimental results. We first look at a sample of pure 8CB, in order to establish the technique. We show that the transition is indeed first order ($t_0>0$) and test the dependence of our measurements on sample thickness. We then study the effects of an applied magnetic field on t_0 and measure t_0 in various 8CB–10CB mixtures.

A. Fluctuations in 8CB

Once we have calibrated the position of the *NA* interface against temperature, we calculate $\zeta(T)$ individually for each isothermal strip parallel to the interface (Fig. 6).

There are three distinct sections to the graph:

(1) Smectic: Here, $\zeta=1\pm2\times10^{-6}$, and the smectic fluctuation level is flat and indistinguishable from the noise.

(2) Nematic: The data here fit a power law of the form

$$\zeta_0+a(T-T^*)^{-\bar{\nu}} \tag{14}$$

with $\zeta_0=0.1\pm1.0\times10^{-6}$, $a=2.10\pm0.01\times10^{-5}$, $T^*=3.7\pm0.4$ mK, and $\bar{\nu}=0.50\pm0.05$. The fit was done over the largest temperature range that still kept the residuals flat (top curve in Fig. 6). T^*, the divergence point of the power law, is identified with the spinodal temperature, while the actual phase transition is located at T_{NA}, which will be determined by fitting, as described below. In Fig. 6, the x axis is $T-T_{NA}$. We will see below that we can fit for the location of T_{NA} in the interfacial region.

(3) Interface: We postulate that the linear region about the transition temperature is the result of an unwanted vertical temperature difference ΔT_z across the sample thickness. We can model the smearing produced by this temperature difference by convolving our model function for ζ with a kernel that mimics the averaging that occurs when one looks through regions of different temperature:

$$\zeta_{meas}(T)=\int_{-\infty}^{\infty}\zeta_{model}(T')K(T-T')dT', \tag{15}$$

where the kernel $K(T-T')$ is given by

$$K(T-T')=\begin{cases}\dfrac{1}{\Delta T_z} & \text{if } -\dfrac{\Delta T_z}{2}<T-T'<\dfrac{\Delta T_z}{2}\\ 0 & \text{otherwise.}\end{cases} \tag{16}$$

$\zeta_{model}(T')$ is given by Eq. (14) for $T'>T_{NA}$ and ζ_0 otherwise.

Some important points are well worth noting here. First, there is an abrupt change in fluctuations at the *NA* transition, quantified by the difference between the transition temperature and the spinodal temperature $T_{NA}-T^*=3.7\pm0.4$ mK [32]. We can characterize this discontinuity by the dimensionless measure

$$t_0=\frac{T_{NA}-T^*}{T_{NA}}=1.2\pm0.1\times10^{-5}. \tag{17}$$

The temperature difference across the sample thickness was calculated to be $\Delta T_z=1.2\pm0.1$ mK.

Second, one notices that the convolution curve fit is systematically off from the data over a small temperature range near the crossover from the nematic section to the interfacial section (around $T-T_{NA}\approx1.4$ mK). The ''rounding'' observed here in the data (see Fig. 6) could be due either to a rounded interface (meniscus) or to a nonlinearity in the vertical temperature gradient.

Finally, we note that the value we obtain for the exponent $\bar{\nu}$ is consistent with that expected [31,10,33] for the bend exponent $\rho_3=-\nu_{parallel}=-0.51$ (we expect $\zeta\propto1/K$: see Appendix A), but not with the twist exponent $\rho_2=(\nu_{parallel}-2\nu_{perp})=-0.35$. Since we have not carried out the more general calculation for ζ with different K's but merely for the single-constant approximation, we do not know the dependence of ζ on K_1, K_2, and K_3. Moreover, while our confidence levels in $\bar{\nu}$ will allow distinguishing between 3D *XY* and tricritical exponents, they are not good enough to distinguish more subtle effects of anisotropy and the extent of crossover. (The main reason is that we do not measure the fluctuations over a large enough range in reduced temperature. Such measurements are not needed for an accurate determination of t_0, our main goal.)

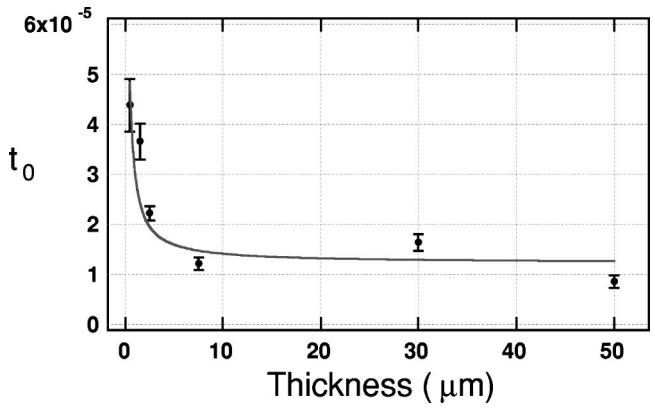

FIG. 7. The first-order discontinuity t_0 is roughly constant for thick samples ($L=7.5$, 30, and 50 μm) but increases for the thin sample 0.5 μm$<L<$2.5 μm. The data are fit to the form $t_\infty+k/L$.

In general, we found that our measurements for 8CB had roughly 10% statistical error but had a sample-to-sample variation as high as 25%. This compares favorably with Cladis's technique, which had errors of about 50% for pure 8CB [15]. For both techniques, the errors were smaller for 8CB–10CB mixtures, where the t_0 discontinuity was larger.

B. The effect of varying sample thickness

To try to understand the origins of the systematic variations we measured in t_0, we examined the effect of varying the sample thickness. On a more fundamental level, we wished to explore whether an anchoring field could, in principle, play a role similar to a magnetic field in suppressing nematic director fluctuations. The magnetic field sets a length scale, the magnetic coherence length ξ_H. We expect to see magnetic-field effects when $\xi_H \approx \lambda$, where λ is a penetration length. Similarly, we expect to see some suppression of fluctuations when the sample thickness $L \approx \lambda$.

There are, however, complications: First, the magnetic field is a clean bulk effect, while the anchoring field is stronger at the surface and is thus intrinsically nonuniform. Second, because the expected critical field is small, the magnetic field has a weaker effect on smectic fluctuations than on nematic director fluctuations. The anchoring field suppresses the smectic fluctuations to the same order, and is thus likely to be a less sensitive test of the HLM effect. Finally, as one goes to thinner samples, finite-size effects should round off the transition, whether first order or second order and convert it to a crossover. It is not clear whether this effect would in principle be separable from the effect on the nematic director fluctuations.

We explored thickness effects by preparing a wedge-shaped sample, where the thickness L varied slowly from about 0.5 to 2.5 μm. We also compiled measurements for constant-thickness samples with $L=7.5$, 30, and 50 μm. We found that while t_0 was roughly constant for samples 7.5 μm thick or greater, it increased sharply for thinner samples (Fig. 7).

One possible explanation for the increase in t_0 is that the anchoring directions imposed by the two glass plates are not perfectly aligned, giving rise to a director twist through the sample, the effects of which become more and more important as the sample thickness decreases. The twist imposed would vary from sample to sample, but its effect can be explored systematically in the wedge sample discussed above. If we assume that boundary conditions at the plates impose a twist, then the situation is analogous to a cholesteric–smectic-A transition, which is always first order. The discontinuity at a cholesteric–smectic-A transition is [34]

$$t_0 = \sqrt{\frac{2K_2 u}{\alpha^2}} q_0 \equiv l_t q_0, \tag{18}$$

where $u=|u_0|(x-x^\star)$ and $\alpha=r/t$ are the quartic and the temperature-independent part of the quadratic Landau coefficients, respectively, and where l_t has units of length. An imposed twist of $\Delta\theta$ corresponds to a cholesteric pitch $q_0=\Delta\theta/L$. Adding the "intrinsic" discontinuity t_∞ that exists in the absence of twist, we thus expect

$$t_{0d} = t_\infty + \frac{\Delta\theta l_t}{L}. \tag{19}$$

The fit to the wedge-sample data in Fig. 7 gives $t_\infty = 1.2 \pm 0.4\times10^{-5}$, well within the systematic errors for samples with thickness ranging from 7.5 μm to 50 μm. The second coefficient gives $\Delta\theta l_t = 1.8\pm0.4\times10^{-5}$ μm. Using $K_2 \approx 2\times10^{-6}$ dyne, $u/\alpha^2 \approx 10^{-8}$ cm^2/dyne, we estimate $l_t \approx 1.4$ nm and, hence, a plate misalignment $\Delta\theta \approx 0.7° \pm 0.2$, which is reasonable given the way we assembled the sample.

From a practical point of view, with respect to studying the HLM transition, we conclude that one should study samples thicker than about 5 μm and that one must take care to align the anchoring directions of the two glass plates.

In conclusion, our measurements of t_0 are not affected by the finite sample thickness or by any plate misalignment. While the origin of the systematic variations in ζ that motivated the thickness study remain unclear, a likely candidate are uncontrolled temperature gradients. Our model of a uniform vertical gradient is probably too crude, and improvements to our apparatus that diminish these gradients will perhaps reduce this source of error.

C. Magnetic-field measurements

Magnetic-field effects at the transition were probed by placing the entire experimental apparatus between the poles of a transverse magnet. Initial runs were done at 1.5 T, but the magnet was unable to provide such fields for long times without damage to the power supply. Later runs were limited to 1.2 T. Contrary to expectations, we saw no suppression of the fluctuations within 50 mK of the transition point and hence no shift in t_0. The zero field and 1.2 T data sets shown in Fig. 8 superpose within statistical errors.

This null measurement implies a lower bound on the critical field H_c. Using the relation for $t_0(H)$ for small H, we have

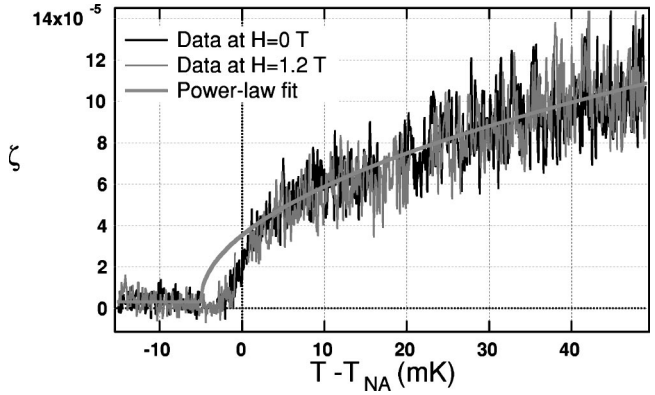

FIG. 8. Effect of magnetic field on 8CB critical behavior. Black data: 0 T. Gray data: 1.2 T. The data (from a single difference image with no averaging) are fit to the exponent $\bar{\nu}=0.5$ (gray fit line). $L=30$ μm and $G=0.59\pm0.02$ K/cm.

$$H_c=\frac{mHt_0}{t_0-t_0(H)}=\frac{(2.17\pm0.01)Ht_0}{t_0-t_0(H)}\approx 21.7\times 1.5\ \text{T},=33\ \text{T}. \tag{20}$$

Here, we have used $H_{max}=1.5$ T, and $[t_0-t_0(H)]/t_0=0.1$, since we would be able to observe a 10% change in t_0. Thus, the experimentally determined lower bound on the critical field is two to three times the prediction based on the HLM mechanism.

One might worry whether a null effect is not due to a problem in the experimental technique itself; however, deep in the nematic, we do see a field-induced suppression of the fluctuations. Plotting ζ vs H [see Fig. 9(a)], we find that this depression is consistent with a quadratic dependence on the field $\zeta=\zeta_0-g_H H^2$. The temperature dependence of the coefficient g_H is shown in Fig. 9(b). The reduction in the field effect near T_{NA} results from the divergence of the twist and bend elastic constants at the transition. Since the magnetic coherence length $\xi_H=(K/\chi_a)^{1/2}1/H$, one reasonably expects the field dependence to be a function of ξ_H; i.e., that $g_H \propto 1/K\propto(T-T_{NA})^{\bar{\nu}}$. The data are consistent with $\bar{\nu}=0.5$, the exponent used to fit ζ.

We repeated the field measurements on a mixture of 8CB–10CB, with concentration chosen to be close to the Landau tricritical point (LTP). Although the zero-field t_0 is higher, the HLM calculation is on firmer ground at the LTP; thus, one might hope that the critical field is closer to the HLM prediction. But once again, we observed no effect. As in Fig. 9, the coefficient g_H goes to zero at T_{NA} in a way consistent with a $\bar{\nu}=0.5$ power law.

D. Variation of t_0 in 8CB–10CB mixtures

Having observed no magnetic-field dependence of t_0, we turned to the 8CB–10CB system, to explore more carefully the magnitude of the HLM effect as a function of nematic range. We also wished to check whether the IFM technique gave results that agreed quantitatively with those from other techniques (calorimetry, front velocity). Expressing measurements in terms of the discontinuity t_0 allows one to compare

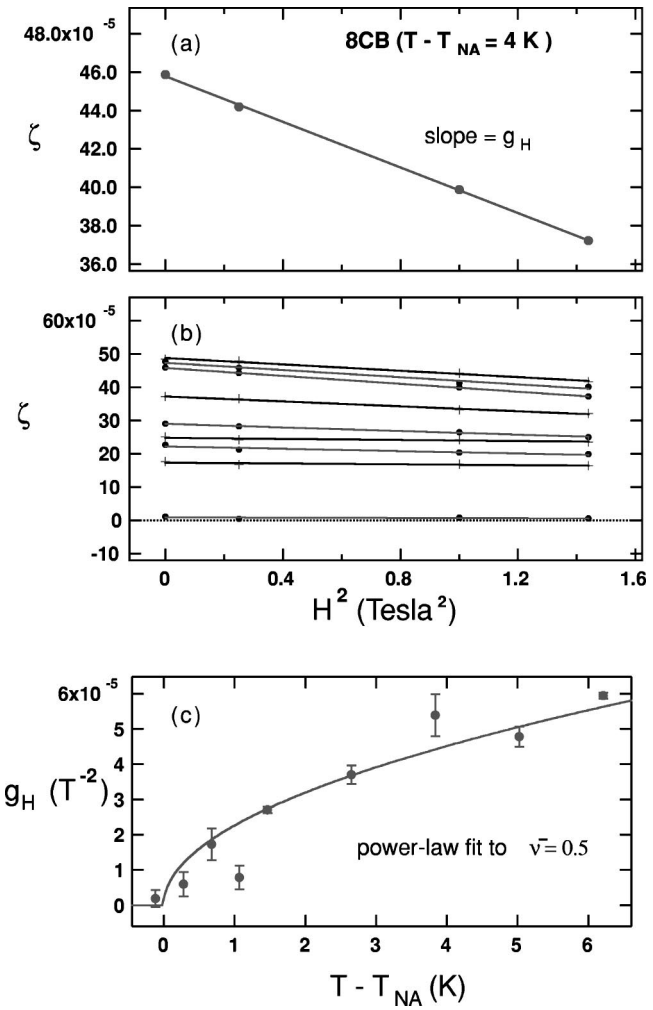

FIG. 9. Variation of fluctuations ζ with magnetic field H at (a) $T-T_{NA}=4$ °C and (b) at 6.2, 5.0, 3.8, 2.6, 1.5, 0.7, 0.3, and -0.1 °C (top to bottom). (c) Field-suppression coefficient g_H near the NA transition.

quantitatively the results of different techniques. In our case, an additional advantage is that in practice, our t_0 measurements are limited to samples with very small discontinuities. Combining our measurements with others allows a larger range of t_0 variation to be explored. (The limitation arises from the need to use a temperature gradient in order to have enough points to measure the discontinuity accurately.)

We have already measured the fluctuations in pure 8CB and in a mixture of concentration $x=0.41$ mole-fraction 10CB in 8CB (at the LTP). We also studied several other mixtures in the range $0<x<0.44$, the largest discontinuity we were able to measure accurately. The measurements $t_0(x)$, shown in Fig. 10 and Table I, can be used to give the phenomenological Landau parameters. We summarize briefly below.

In Eq. (3), above, there are four free parameters. The values of two of them, $r=\alpha[(T-T^*)/T^*]$ and w, have been determined in previous work [35,16]. From the solution to the simultaneous equations $f=0$ and $df/d\psi=0$, we can derive relations between the Landau parameters. The order parameter ψ depends on the Landau parameters via the cubic

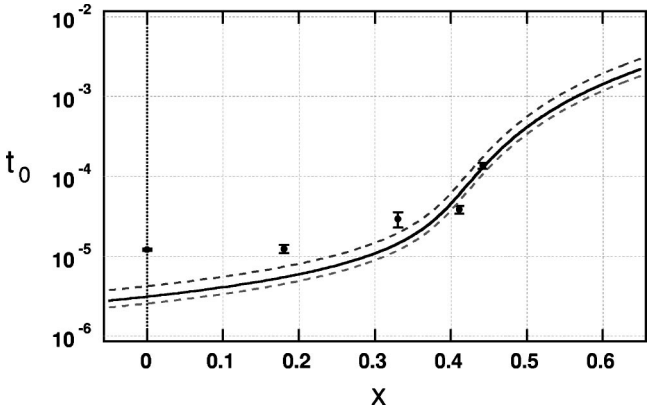

FIG. 10. Fit of t_0 data (this work) to the Anisimov parameters, with u_0 as an additional fit parameter. Top and bottom dashed curves show fits to t_0 for $\bar{\nu}=0.6$ and $\bar{\nu}=0.4$, respectively. (The data points for these exponent values are not shown.)

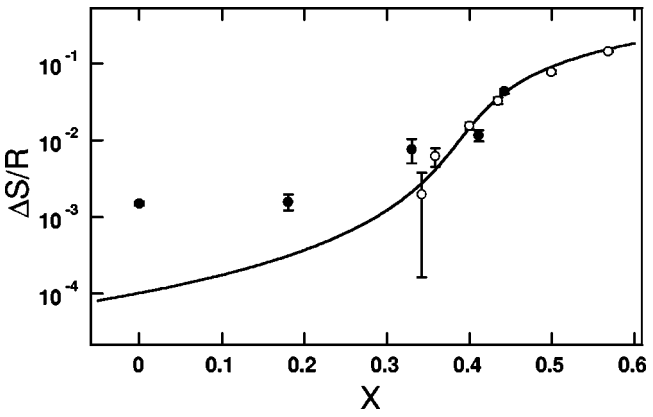

FIG. 11. Entropy-jump estimate based on the fitted Landau parameters. Also shown is the HLM fit and the calorimetry data of Marynissen *et al.* [13].

equation, $\psi^3+(3u/4E)\psi-w/2E=0$.

Both $\Delta S/R$ and t_0 can be related to the phenomenological Landau parameters, r, w, u, and E. Previous experiments measured scaled latent heats; in the approximation $E=1$, u is scaled away. Near the Landau tricritical point, u is written as $u=u_0(x-x^*)$ where x^* was also determined in the previous experiments. The scaled latent heats are insensitive to u_0 (although the unscaled ones are). Analysis [35] of previous experiments determined the two parameters $\Delta S^*/R=0.0261$ and $\beta=(-3/8)(\alpha u_0/E)=0.993$, in addition to x^*.

In the present experiment, we measure directly $t_0=r(T_{NA})/\alpha$. Using the simultaneous equations $f=0$ and $df/d\psi=0$, r depends on w, u_0, and E, while the parameter α is a function of u_0/E only. Also, $\Delta S^*/R=\alpha(w/4E)^{2/3}$. These equations give us both α and w as a function of u_0 and E. Here, we use the values determined in analysis of previous experiments [35] for $\Delta S^*/R$ and β. We can then similarly compute $\Delta S/R=\alpha\psi^2$.

In addition, the exponent of the power law $\bar{\nu}$ in all cases was held fixed to $\bar{\nu}\approx 0.5$, which was close to the value obtained from a free fit. In a free fit, there was always an uncertainty of $\approx\pm 0.1$ in the value of $\bar{\nu}$. Forcing the fits with an exponent $\bar{\nu}=0.4$ and $\bar{\nu}=0.6$ systematically *reduces* and *increases* the value, respectively, of t_0 for all samples. The magnitude of this variation due to the choice of exponents is shown by the dashed lines in Fig. 10. The qualitative nature of the dependence described above is, however, unchanged. Because u_0 only shifts the HLM predictions up and down, there is a qualitative and systematic disagreement between the HLM fit and the data.

TABLE I. t_0 for different mixture concentrations, with $\bar{\nu}=0.5$. The first errors quoted are statistical, while the second are systematic variations from sample to sample. The latter do not affect the magnetic-field measurements.

Concentration x	Discontinuity t_0
0	$1.21\times10^{-5}\pm0.10\pm0.4$
0.18	$1.24\times10^{-5}\pm0.15\pm0.4$
0.33	$2.9\times10^{-5}\pm0.6\pm0.4$
0.41	$3.8\times10^{-5}\pm0.4\pm0.4$
0.44	$13.6\times10^{-5}\pm1.1\pm0.4$

We use the parameter set deduced by Anisimov *et al.* to calculate ψ and r, from which we can calculate $t_0\equiv r/\alpha$. We fit for u_0 and E. The exponent is fixed at $\bar{\nu}=0.5$. We get $u_0=-0.79\pm0.03$ and $E=0.97\pm0.03$. These are both of order one, as expected. The error bars on a free fit without the exponent held are ±0.1. In Fig. 10, we show fits to the HLM theory where the exponent $\bar{\nu}$ is held at 0.5 (and, in dashed lines 0.4 and 0.6). The corresponding values of u_0 in the three fits are -0.74, -0.79, and -0.88, all ±0.03.

Given a value of u_0, one can then calculate the corresponding latent heat, as shown in the entropy-jump plot in Fig. 11. We also add the latent heat data of Marynissen *et al.* [13]. In particular, the calculated entropy change per mole for 8CB is $\Delta S/R\approx10^{-3}$.

Close to the LTP, the zero-field data from the 8CB–10CB mixtures (closed circles in Fig. 10) are consistent with that of Marynissen *et al.* [13] (open circles in Fig. 10); in this region, it is also consistent with predictions based on HLM theory (solid fit line in the same figure) using the phenomenological Landau parameters of Anisimov *et al.* [35]. However, for smaller x, the discontinuity is systematically *larger* than the HLM-predicted value.

We tried to account for this by allowing for a quadratic correction to the dependence of the quartic coefficient

$$C=C_0(x-x^\star)+C_1(x-x^\star)^2. \tag{21}$$

Refitting the data now over the whole range of x, we find $C_1>C_0$, which is not reasonable given that the linear term alone works well for $0<(x-x^\star)\lesssim0.2$. Moreover, the fit becomes much worse over the large-x range that was previously well fit. As a second attempt, we allow the sixth-order

coefficient E to vary. This does not change the shape of the curve significantly, and the data are still poorly fit over the entire range, whatever value we take for E. We conclude that the discrepancy with HLM for the small-x data cannot be fixed by either of these modifications to the original curve fits. The measured t_0 is truly higher than the value predicted by HLM.

V. CONCLUSIONS AND PROSPECTS

We have introduced and characterized a sensitive new technique, IFM, for probing long-wavelength fluctuations in liquid-crystal systems. We can anticipate that this technique will be valuable for free-film studies (where the free boundary conditions simplify the calculations of fluctuations) and in other, more exotic phases (Sm C, ferroelectrics, etc.). In the present case of the NA transition, the method is sensitive enough to clearly establish that the transition in 8CB is first order, even though the difference between equilibrium transition and the spinodal is less than 4 mK.

We showed that t_0, while constant for thick samples, increases markedly for thinner samples. We argue that small sample-plate misalignments, which lead to an overall twist in the nematic, are responsible. The reasoning is the same for concluding that the cholesteric–smectic-A transition must always be first order. As a practical matter, such misalignment can introduce artifacts in measurements near the NA transition, for very thin samples. Such artifacts would be present in measurements of other quantities (latent heat, etc.), as well.

Our main results are two tests of the predictions of the Halperin-Lubensky-Ma theory of the NA transition. The first is that the discontinuity should be reduced and eventually eliminated by adding a magnetic field along the director. We find no such effect, although we do see the usual field suppression of fluctuations. Because the material parameters of our liquid crystals are well known, we can conclude that the ''tricritical'' field (where the transition becomes second order) is at least three times higher than the HLM prediction of 10 T. A very recent experiment by Lelidis examines the effect of an applied electric field [36]. He gives evidence for a tricritical point at a field of about 13 V/μm, which corresponds to a critical magnetic field of about 130 T, consistent with our results.

Second, we measure the concentration dependence of t_0 in an 8CB–10CB mixture. For concentrations where the nematic range is very small, our results agree with both previous measurements and with the HLM predictions. But for concentrations with larger nematic range, there is a systematic deviation, with the observed t_0 as much as five times larger than the predicted value. Thus both experimental tests of the HLM predictions lead to serious discrepancies.

An obvious candidate to explain the discrepancies is smectic fluctuations, which become more and more important as the nematic range is increased and which are neglected in the HLM calculation. One's naive intuition, though, is that because smectic fluctuations eventually drive the transition second order, the HLM prediction should be progressively larger than experiment. We observe the reverse.

Recently, however, Herbut *et al.* have extended the HLM calculation to include smectic fluctuations as a perturbation [37]. The calculation, which is done in the context of the superconductivity free energy, shows that, surprisingly, the renormalization of parameters caused by gauge fluctuations makes a material effectively more type I. For the NA transition, this means that the nematic range is renormalized to be smaller than its ''bare'' value, increasing the predicted t_0. Herbut *et al.* then show that, at the cost of introducing a cutoff parameter, one can fit $t_0(x)$ over the entire concentration range.

As for future work, one can envision several different directions. The sensitivity of the IFM technique was, in our case, limited by uncontrolled static temperature gradients that blurred the interface image. If these stray gradients can be reduced, systems with smaller t_0 would be accessible. By starting from a material with smaller zero field t_0 than 8CB, one might be able to see external field effects with a magnetic field [38].

Whether by electric or magnetic fields, it would be extremely interesting to probe critical behavior in the vicinity of the postulated tricritical point. Likewise, it would be interesting to measure apparent critical exponents in the presence of an external field. In this context, we notice in a review [7] of critical exponents that the correlation-length exponent $\xi_\parallel$ has a maximum for $T_{NA}/T_{IN} \approx 0.8$. It is tempting to speculate whether this maximum is associated with a tricritical point. Extending the t_0 measurements to materials and mixtures with yet larger nematic range could allow one to probe the concentration dependence all the way to the tricritical point.

Note added in proof. Professor C. W. Carland has pointed out that in [11], J. Thoen, H. Marynissen, and W. van Dael claim an upper limit to the entropy jump for pure 8CB that is equivalent to $\Delta S/R = 1.6 \times 10^{-4}$. This would be consistent with the HLM prediction, as graphed in Fig. 11, but would be inconsistent with the zero-field measurement of 8CB and the magnetic-field limit reported here. It is also inconsistent with the recent electric-field measurement of Lelidis [36] which, like the other measurements, implies an entropy jump about ten times higher than the calorimetry result. At present, we do not understand the origin of these inconsistencies.

ACKNOWLEDGMENTS

This work was supported by NSERC (Canada). We are grateful to P. Cladis, M. Wortis, M. Plischke, P. Lammert, and C. W. Garland for helpful discussions. We thank B. Heinrich for generous access to his magnet.

APPENDIX A:

In this appendix, we give a more thorough treatment of the optics of a fluctuating nematic film, as observed through

a microscope. Galatola has developed a systematic formalism for treating such a situation, which in principle can be adapted to our case [39]. Although such a treatment poses no conceptual problem, the formalism is rather complex. Here, we limit ourselves to a simpler calculation, whose goals are more modest. As mentioned in the text, the approximation of the planar nematic as a fluctuating waveplate is adequate for most of our purposes. We need to go beyond such a treatment only to account for two observations: first, the waveplate approximation leads to the wrong form for the angular dependence for the variance $\zeta(\theta)$ [Eq. (13)]. Second, we want to make explicit the dependence of ζ on the nematic elastic constants, in order to justify the expected scaling near the *NA* transition. Finally, we discuss briefly the effects of sample thickness.

We start by considering the propagation of light through a fluctuating nematic liquid-crystalline film in a direction z perpendicular to the film. We assume the light to be monochromatic, neglect diffraction effects, and consider the effects of perturbations to the director orientation $\delta\mathbf{n}$. For plane waves that propagate along z, at lowest order, only in-plane director fluctuations in the sample plane contribute to intensity fluctuations of the outcoming light. Thus, it suffices to represent the electromagnetic field purely by the electric-field amplitude $\vec{E}=(E_x,E_y)$ of a plane wave propagating along the z direction. We write

$$\vec{E}_{\rm out}=\mathbf{T}\vec{E}_{\rm in}, \tag{A1}$$

where $\mathbf{T}$ is the 2×2 transfer matrix [40]). The E component of the incoming electromagnetic field is $\vec{E}_{\rm in}e^{i\omega t}$ and that of the outgoing electromagnetic field is $\vec{E}_{\rm out}e^{i\omega t}$. The transfer matrix of the system takes the form

$$\mathbf{T}=\mathbf{P_1}\mathbf{R}\mathbf{D}\mathbf{R}^{-1}\mathbf{P_2}, \tag{A2}$$

with

$$\mathbf{P}_1=\begin{pmatrix}1&0\\0&0\end{pmatrix},\quad \mathbf{P}_2=\begin{pmatrix}0&0\\0&1\end{pmatrix},\quad \text{and}\quad \mathbf{R}=\begin{pmatrix}\cos\theta&\sin\theta\\-\sin\theta&\cos\theta\end{pmatrix}, \tag{A3}$$

representing the two polarizers and the rotation matrix, θ being the angle between the average director orientation in the film and the first polarizer axis. Then $\mathbf{D}$ is the transfer matrix of a nematic film aligned along the x axis. In the absence of fluctuations,

$$\mathbf{D}^{(0)}=\begin{pmatrix}e^{iL\gamma/2}&0\\0&e^{-iL\gamma/2}\end{pmatrix}, \tag{A4}$$

where $\gamma=2\pi\Delta n/\lambda$ is the phase difference introduced between the two polarizations (along and perpendicular to the director) per unit length, Δn is the birefringence, λ the wavelength, and L the film thickness. Thus, ignoring fluctuations,

with

$$\mathbf{T}^{(0)}=\begin{pmatrix}0&\alpha_0\\0&0\end{pmatrix}, \tag{A5}$$

where $\alpha_0=-i\sin(2\theta)\sin(\gamma L/2)$. Note that the transmitted intensity $I_{in}|\alpha_0\alpha_0^*|$ reproduces Eq. (10), above.

Next, we consider the effect of nematic fluctuations. Imagine slicing the film into N infinitesimal layers of thickness $t=L/N$, and take the limit $N\to\infty$. The total transfer matrix is

$$\mathbf{D}=\mathbf{D_1}\mathbf{D_2}\ldots\mathbf{D_j}\ldots\mathbf{D_N}, \tag{A6}$$

where $\mathbf{D}_j=\mathbf{D}_j^{(0)}+\delta\mathbf{D}_j$ is the transfer matrix of the jth slice, with $\delta\mathbf{D}_j$ the director fluctuations of the jth slice and $\mathbf{D}_j^{(0)}=\mathbf{D}_1^{(0)}$ for all j. The lowest-order contribution, which corresponds to single scattering, is

$$\mathbf{D}=\mathbf{D}^{(0)}+\sum_j(\mathbf{D}_1^{(0)})^{j-1}\delta\mathbf{D}_j(\mathbf{D}_1^{(0)})^{N-j}. \tag{A7}$$

Higher-order terms correspond to multiple-scattering effects, which we ignore.

Director fluctuations can either be along the film or perpendicular to it. For propagation strictly along the z direction, perpendicular fluctuations are second order and can be neglected. Below, we will consider the effect of light that is scattered at an angle with respect to z. For now, we consider the in-plane director fluctuations. Let $\delta\theta_j$ represent the angular deviation of the director in layer j from the average director orientation θ. To lowest order,

$$\delta\mathbf{D}_j=\begin{pmatrix}0&-i\gamma t\,\delta\theta_j\\-i\gamma t\,\delta\theta_j&0\end{pmatrix}. \tag{A8}$$

Inserting this into Eq. (A7), we find that

$$\delta\mathbf{D}=\sum_j\begin{pmatrix}0&\exp[i(N+1-2j)\gamma t/2]i(\gamma t/2)\,\delta\theta_j\\\exp[-i(N+1-2j)\gamma t/2]i(\gamma t/2)\,\delta\theta_j&0\end{pmatrix}, \tag{A9}$$

where $\mathbf{D}=\mathbf{D}^{(0)}+\delta\mathbf{D}$. Finally, the correction to the transfer matrix is given by

$$\delta\mathbf{T}=\begin{pmatrix}0 & \alpha_1\\ 0 & 0\end{pmatrix} \tag{A10}$$

$$\begin{aligned}\alpha_1 &= i\frac{\gamma t}{2}\sum_j \delta\theta_j\{\cos^2\theta\exp[i(N+1-2j)\gamma t/2]\\ &\quad -\sin^2\theta\exp[-i(N+1-2j)\gamma t/2]\}\\ &\approx i\frac{\gamma}{2}\int_0^L dz\,\delta\theta(z)[\cos^2\theta\, e^{i(L-2z)\gamma/2}-\sin^2\theta\, e^{-i(L-2z)\gamma/2}]\\ &= i\frac{\gamma}{2}\int_0^L dz\,\delta\theta(z)\{\cos 2\theta\cos[(2z-L)\gamma/2]\\ &\quad + i\sin[(L-2z)\gamma/2]\}.\end{aligned} \tag{A11}$$

The transmitted intensity is then

$$I=I_{\rm in}(|\alpha_0+\alpha_1|^2)\approx I_{\rm in}(|\alpha_0|^2+\alpha_0^*\alpha_1+\alpha_0\alpha_1^*). \tag{A12}$$

Thus, to lowest order, the resulting variance in intensity fluctuations is

$$\begin{aligned}\langle I^2\rangle-\langle I\rangle^2 &= I_{\rm in}^2\gamma^2\sin^2 4\theta\sin^2(\gamma L/2)\int_0^L dz_1\int_0^L dz_2\\ &\quad\times\cos[(2z_1-L)\gamma/2]\cos[(2z_2-L)\gamma/2]\\ &\quad\langle\delta\theta(x,y,z_1)\,\delta\theta(x,y,z_2)\rangle.\end{aligned} \tag{A13}$$

This gives us the lowest-order relation between director fluctuations and intensity fluctuations. Note that while $\delta\theta$ depends on x and y, the correlation function $\langle\delta\theta^2\rangle$ does not, since the sample is laterally homogeneous. Note, too, the $\sin^2 4\theta$ term, which matches Eq. (13).

To proceed further, we need to put in the elasticity laws for the nematic, which govern the $\delta\theta$ fluctuations. We make the ''one-constant'' approximation, where the three elastic constants of the nematic are taken to be equal: $K_1=K_2=K_3=K$. In this approximation,

$$\begin{aligned}\langle\delta\theta(x,y,z_1)\,\delta\theta(x,y,z_2)\rangle &= \int dq_x\,dq_y G(q_x,q_y;z_1,z_2)=\frac{k_BT}{L}\sum_n\int dq_x\,dq_y\frac{\sin(nz_1\pi/L)\sin(nz_2\pi/L)}{K[q_x^2+q_y^2+(n\pi/L)^2]}\\ &= \frac{\pi k_BT}{KL}\sum_n\log\left[1+\left(\frac{L\Lambda}{2n\pi}\right)^2\right]\sin(nz_1\pi/L)\sin(nz_2\pi/L),\end{aligned} \tag{A14}$$

where Λ is the upper cutoff of q_x and q_y, which in this case should be taken to be $2\pi/a$ with a being the pixel size, around one micron. In Eq. (A14), the Green's function has been expanded in terms of eigenfunctions that are periodic in the x and y directions and vanish at $z=0$ and L. Thus,

$$\langle I^2\rangle-\langle I\rangle^2=I_{\rm in}^2\gamma^2\sin^2 4\theta\sin^2(\gamma L/2)\frac{\pi k_BT}{KL}\sum_n\log\left[1+\left(\frac{L\Lambda}{2n\pi}\right)^2\right]\mathcal{I}_n^2, \tag{A15}$$

where

$$\mathcal{I}_n=\int_0^L dz\cos[(2z-L)\gamma/2]\sin(n\pi z/L)=\frac{2n\pi/L}{(n\pi/L)^2-\gamma^2}\cos(L\gamma/2), \tag{A16}$$

for odd n and 0 for even n. Thus,

$$\begin{aligned}\langle I^2\rangle-\langle I\rangle^2 &= I_{\rm in}^2\left(\frac{\pi\gamma^2Lk_BT}{K}\right)\sin^2 4\theta\sin^2(\gamma L)\sum_n\\ &\quad\times\log\left[1+\left(\frac{L\Lambda}{2n\pi}\right)^2\right]\frac{1}{(n\pi)^2}\left(\frac{1}{\left(\frac{\gamma L}{n\pi}\right)^2-1}\right)^2,\end{aligned} \tag{A17}$$

where the sum is over odd n. The important length scales are $L\approx 30\ \mu$m (most of our measurements used this thickness) and $\gamma^{-1}\approx 0.7\ \mu$m.

In the sum [Eq. (A17)] the major contribution comes from the term with $n\pi$ closest to $\gamma L\approx 48$ (i.e., from $n=15$). Qualitatively, it is easy to understand why a term that is neither too big nor too small dominates. The contribution from the lowest-order terms vanishes because of the adiabatic effect: the polarization is simply rotated along with the nematic. Because $\delta\theta$ vanishes at the top and bottom sample plates, there is no overall birefringence effect. On the other hand, modes that vary too rapidly will be averaged over by the longer wavelength of the light and thus also give only a small contribution. In between, for intermediate scales, lies the maximum.

We have so far ignored the main complication that arises

due to the optics; light is collected over a range of angles ϕ from the z axis, where ϕ can be as large as 20°. Imagine a ray passing through the film making an angle ϕ with the z axis. A fluctuation $\delta\phi$ in the nematic direction perpendicular to the film now contributes changes $E_{\rm out}$ by order $\delta\phi \sin 2\phi$. The basic idea is that perpendicular fluctuations of the director add an extra phase difference between the ordinary and extraordinary ray which goes as $\Delta n \sin 2\phi$. Here, Δn is the birefringence of the liquid crystal, averaged to take into account the azimuthal variation in the effective δn, since the entire cone of rays coming out at an angle ϕ are collected. This reduces the bare Δn by $\approx 1/3$.

To estimate the effects of these out-of-plane fluctuations, we once again carry out the prescription of slicing up the film into layers and, using Eq. (A7), obtain the lowest-order contribution of fluctuations to the transfer matrix. Now,

$$\delta \mathbf{D}_{\perp,j} = \begin{pmatrix} i(\delta\Phi)_j & 0 \\ 0 & -i(\delta\Phi)_j \end{pmatrix}, \tag{A18}$$

with $\delta\Phi$ being the extra phase difference introduced between the ordinary and extraordinary rays as a result of the deviation of the director from the XY plane. [Compare with Eq. (A8).] We then can estimate the contribution of perpendicular director fluctuations to the intensity variance:

$$I_{\rm in}^2 \gamma^2 \sin^4 2\theta \sin^2(\gamma L/2)\cos^2(\gamma L/2)\mathcal{J}_\perp \times \sin^2 2\phi \int_0^L dz_1 \int_0^L dz_2 \langle \delta\varphi(x,y,z_1)\delta\varphi(x,y,z_2)\rangle, \tag{A19}$$

where $\delta\varphi(x,y,z)$ is the out-of-plane director fluctuation at the point (x,y,z). Note again that $\langle \delta\varphi^2\rangle$ is independent of x and y. Note the $\sin^4 2\theta$ angular dependence. In Eq. (A19), $\mathcal{J}_\perp$ is a dimensionless factor that depends on the detailed optics; it seems reasonable to assume it to be order unity. We interpret ϕ here as the maximum ray angle collected and absorb the overall intensity dependence of $I(\phi)$ into $\mathcal{J}_\perp$.

To attempt to evaluate a, we use the one-constant approximation, as before, and follow Eqs. (A13)–(A17), with $\mathcal{I}_n$ now being the integral

$$\mathcal{I}_n = \int_0^L dz \sin(n\pi z/L). \tag{A20}$$

Thus, we finally obtain

$$\langle I^2\rangle - \langle I\rangle^2 = I_{\rm in}^2 \mathcal{J}_\perp \left(\frac{\pi\gamma^2 L k_B T}{K}\right) \sin^4 2\theta \sin^2(\gamma L)\sin^2 2\phi \times \sum_n \log\left[1+\left(\frac{L\Lambda}{2n\pi}\right)^2\right]\frac{1}{(n\pi)^2}, \tag{A21}$$

where the summation is again over odd values of n. Again, the approximations made (including the unknown geometric factor), make this result more qualitative than quantitative.

Adding the two variances and noting that $\sin^4 2\theta = \sin^2 2\theta - \frac{1}{2}\sin^2 4\theta$, we find

$$\hat{\zeta}(\theta) = a \sin^2 2\theta + b \sin^2 4\theta, \tag{A22}$$

which matches the experimental result [Fig. 4(b)].

The structure of the sums in Eqs. (A17) and (A21) give some hint as to why the coefficients a and b of the two terms may be comparable. The azimuthal term b is reduced because of the adiabatic transport effect. The leading term ($n=3$) is roughly 10 times smaller than the $n=1$ term. On the other hand, the out-of-plane term a is reduced by the factor $\sin^2 2\phi$. As there is no adiabatic transport of the polarization, which is a rotation effect, the $n=1$ term dominates here. Thus, at least loosely speaking, it is plausible that the terms are of comparable order. Finally, it is encouraging that the experimental form for $\hat{\zeta}(\theta)$ fits Eq. (A22), in that it implies that higher-order terms (e.g., $\langle \delta\theta^4\rangle$ or $\langle \delta\varphi^4\rangle$) are negligible.

Our other goal was to understand the critical behavior of ζ. Here, we see that in the one-constant approximation, $\zeta \propto K^{-1}$.

Finally, one sees that ζ is a complicated function of the sample thickness L. Roughly, $\zeta \propto L$, but modulated with the same period as $\langle I\rangle$. While the data in Fig. 5(b) follow this trend, multiple scattering in the thicker sample regions makes our result only qualitative.

[1] P. Pfeuty and G. Toulouse, *Introduction to the Renormalization Group and to Critical Phenomena*, 1st ed. (Wiley-Interscience, Chichester, 1978).

[2] C. Itzykson and J. B. Zuber, *Quantum Field Theory* (McGraw Hill, NY, 1980), pp. 612–614.

[3] B. I. Halperin, T. C. Lubensky, and S. K. Ma, Phys. Rev. Lett. **32**, 292 (1974).

[4] P. G. de Gennes, Solid State Commun. **10**, 753 (1972).

[5] T. C. Lubensky, J. Chim. Phys. **80**, 32 (1983).

[6] P. G. de Gennes and J. Prost, *The Physics of Liquid Crystals*, 2nd ed. (Clarendon, Oxford, 1993).

[7] C. W. Garland and G. Nounesis, Phys. Rev. E **49**, 2964 (1994).

[8] W. L. McMillan, Phys. Rev. A **4**, 1238 (1971).

[9] There is a formal analogy [4] between the Landau-deGennes free energy for smectics and the Landau-Ginzburg free energy for superconductors. Small nematic ranges correspond to strong type-1 superconductors, while large nematic ranges should correspond to type-2 superconductors. While this analogy has been very powerful in gaining an intuition for the *NA* transition, it neglects anisotropy; in liquid crystals, the splay elastic term explicitly breaks gauge symmetry.

[10] D. Brisbin, R. DeHoff, T. E. Lockhart, and D. L. Johnson, Phys. Rev. Lett. **43**, 1171 (1979).

[11] J. Thoen, H. Marynissen, and W. Van Dael, Phys. Rev. A **26**, 2886 (1982).

[12] J. Thoen, H. Marynissen, and W. Van Dael, Phys. Rev. Lett. **52**, 204 (1984).

[13] H. Marynissen, J. Thoen, and W. Van Dael, Mol. Cryst. Liq. Cryst. **124**, 195 (1985).
[14] M. A. Anisimov, V. P. Voronov, E. E. Gorodetskii, and V. E. Podnek, JETP Lett. **45**, 425 (1987).
[15] P. E. Cladis, W. van Saarloos, D. A. Huse, J. S. Patel, J. W. Goodby, and P. L. Finn, Phys. Rev. Lett. **62**, 1764 (1989).
[16] N. Tamblyn, P. Oswald, A. Miele, and J. Bechhoefer, Phys. Rev. E **51**, 2223 (1995).
[17] N. Tamblyn, M.Sc. thesis, Simon Fraser University, 1994.
[18] A. Yethiraj and J. Bechhoefer, Phys. Rev. Lett. **84**, 3642 (2000).
[19] A. Yethiraj, Ph.D. thesis, Simon Fraser University, 1999.
[20] R. Mukhopadhyay, A. Yethiraj, and J. Bechhoefer, Phys. Rev. Lett. **83**, 4796 (1999).
[21] A. Yethiraj and J. Bechhoefer, Mol. Cryst. Liq. Cryst. **304**, 301 (1997).
[22] Y. Galerne, I. Poinsot, and D. Schaegis, Appl. Phys. Lett. **71**, 221 (1997).
[23] Products K24 and K30, Merck Industries.
[24] We use a Perkin Elmer LS1130 flashpac, with a bulb with 1.5-mm arclength, to limit the source size. We chose a 1-μF discharge capacitor, which provided 0.5 J/flash, a quarter of which is in the visible region. The arc lamp is (nearly) the brightest nonlaser source available. One could use lasers, but their coherence introduces other complications.
[25] G. W. Ellis, J. Cell Biol. **101**, 83A (1985).
[26] Sensys camera, Roper Scientific. The CCD sensor is a Kodak KAF-1400 chip, with 1317 by 1035 pixels, each measuring 6.8-μm square. Readout rate was 1 MHz. Because a large amount of light was available, read and dark noise were negligible; shot noise dominated.
[27] Neslab RTE-110 waterbath, Neslab Instruments Inc.
[28] Xantrex XTD 15-4 power supply, Xantrex Technology Inc.
[29] B. Jaggi, B. Pontifex, J. Swanson, and S. S. S. Poon, SPIE **1901**, 99 (1993).
[30] P. P. Karat and N. V. Madhusudana, Mol. Cryst. Liq. Cryst. **36**, 51 (1976).
[31] D. Davidov, C. R. Safinya, M. Kaplan, S. S. Dana, R. Schaetzing, R. J. Birgeneau, and J. D. Litster, Phys. Rev. B **19**, 1657 (1979).
[32] In an early version of this experiment [21], we had reported a discontinuity of 2 mK. The lower value was obtained because we had not properly accounted for the shot-noise contribution to the intensity fluctuations.
[33] B. M. Ocko, R. J. Birgeneau, and J. D. Litster, Z. Phys. B: Condens. Matter **62**, 487 (1986).
[34] L. Benguigui, Liq. Cryst. **25**, 1 (1998).
[35] M. A. Anisimov, P. E. Cladis, E. E. Gorodetskii, D. A. Huse, V. E. Podneks, V. G. Taratuta, W. van Saarloos, and V. P. Voronov, Phys. Rev. A **41**, 6749 (1990).
[36] I. Lelidis, Phys. Rev. Lett. **86**, 1267 (2001).
[37] I. Herbut, A. Yethiraj, and J. Bechhoefer, Europhys. Lett. **55**, 317 (2001).
[38] The electric-field measurements of Lelidis, which measure directly the nematic birefringence, have the disadvantage that the applied field induces alternating ionic currents. These currents heat the sample, perturbing the temperature stability. One can somewhat circumvent these problems by applying the electric field in short pulses and by accumulating data over many pulses. Magnetic-field measurements, when possible, are a cleaner probe. For a description of the electric-field techniques, see I. Lelidis and G. Durand, Phys. Rev. Lett. **73**, 672 (1994) and also I. Lelidis, Ph.D. thesis, Université de Paris-Sud U.F.R. Scientifique d'Orsay, 1994.
[39] P. Galatola, Phys. Rev. E **49**, 4552 (1994).
[40] The basic transfer-matrix method we use is described in almost any intermediate-level optics text. The application of transfer matrices to the optics of a continually varying nematic may be found in S. Chandrasekhar, *Liquid Crystals*, 2nd ed. (Cambridge University Press, Cambridge, 1992), Ch. 4.